Catalysis Today 155 (2010) 326–330

Contents lists available at ScienceDirect

Catalysis Today

journal homepage: www.elsevier.com/locate/cattod

Flying droplets as model system for spray drying—An *in situ* synchrotron X-ray scattering study on complex oxides catalyst precursors

Jork Leiterer [a], Franziska Emmerling [a,*], Jörg Radnik [b,**], Ursula Bentrup [b], Angelika Brückner [b]

[a] BAM Federal Institute of Materials Research and Testing, Richard-Willstätter-Str. 12, 12489 Berlin, Germany
[b] Leibniz-Institut für Katalyse, Albert-Einstein-Str. 29a, 18059 Rostock, Germany

ARTICLE INFO

Article history:
Available online 26 November 2009

Keywords:
Acoustic levitation
Spray drying
Molybdate catalysts
X-ray scattering

ABSTRACT

As a model for spray drying the early stages of crystallization of complex molybdate catalyst precursors were monitored online in droplets levitated acoustically. Synchron X-ray scattering techniques were applied to study the drying process of a typical molybdate catalysts precursor prepared from Ni-,Fe-,Bi-nitrate, ammonium heptamolybdate and H_3PO_4. Comparison with diffraction patterns obtained from sessile droplets shows significant differences in the crystal growth, whereas the final crystal structure – including a Keggin-type anion – is identical in both cases. The levitated samples exhibit a decelerated growth with a large number of small crystallites at the beginning of the crystallization, whereas in case of the sessile droplets a small number of large crystallites were observed after a few minutes. The acoustic levitation using an ultrasonic trap proves to be an elegant tool to mimic spray drying and offers new possibilities in relation to the understanding of the drying process.

1. Introduction

Molybdate containing mixed metal oxides are widely applied as catalysts in heterogeneous selective oxidation processes [1,2]. In industry, such catalysts are frequently prepared by slurry procedures comprising a series of subsequent steps including precipitation, isolation of the precipitate, spray drying and final calcination. Tailoring the different preparation steps for the preferential formation of desired precursor and catalyst phases would be highly desirable but is mostly difficult to realize, since a sound understanding of the different preparation steps is still missing. Thus, the preparation method, the nature of the used components and the reaction conditions play an important role and affect the final composition, structure and performance of the catalytic material. To optimize the synthesis strategies of such complex oxides, particularly in terms of an enhanced and reproducible performance of the catalysts, a deeper insight into the synthetic process by *in situ* methods is inevitable.

Recently, we reported on simultaneous wide- and small-angle X-ray scattering (WAXS/SAXS) and Raman spectroscopic experiments at the μSpot Beamline (BESSY, Berlin) enlightening the precipitation of certain phases in the liquid phase synthesis of molybdate catalyst precursors [3]. These investigations in the complex system ammonium heptamolybdate (AHM)/Ni-,Fe-,Bi-nitrate/HNO_3/H_3PO_4 showed that after the addition of the mixed metal nitrate solution to the solution of AHM, a crystalline precipitate is immediately formed indicated by the respective Bragg reflections. The precipitate alters after the addition of H_3PO_4, loses its crystallinity and partly dissolves, respectively, at higher temperature. At the end of the experiment no Bragg reflections were detected. The existence of Keggin-type ions could be verified by Raman spectroscopy. If the slurry was spray-dried, the formation of a crystalline phase with cubic symmetry consisting of Keggin ions could be observed.

Obviously, the drying procedure leads to crystallization. Only few investigations on the influence of the drying methods on the catalytic performance and no *in situ* studies to our best knowledge are known. It was reported by Lin [4], that starting from Mo–V–Te–Nb oxide precursors with identical composition, the powder pattern of the dried samples differ depending on the applied drying method (heat evaporation and freeze-dry) [4]. Reflecting the structural differences, the respective catalyst performance varies, too. However, further information about the early stages of drying, especially the crystallization process during the whole drying period, was not given.

In situ investigations of spray-drying processes are very rare. First attempts were made by Sen et al. [5] applying a mobile spray dryer at a synchrotron beamline [5]. The authors derived information on the particle formation probing different temperature zones. The suitability of the acoustic levitation to imitate the condition during the spray-drying was discussed in the literature [6,7]. Particularly, former investigations on the evaporation

* Corresponding author. Fax: +49 30 8104 1137.
** Corresponding author. Fax: +49 381 1281 51308.
E-mail addresses: franziska.emmerling@bam.de (F. Emmerling), joerg.radnik@catalysis.de (J. Radnik).

0920-5861/$ – see front matter © 2009 Elsevier B.V. All rights reserved.
doi:10.1016/j.cattod.2009.11.001

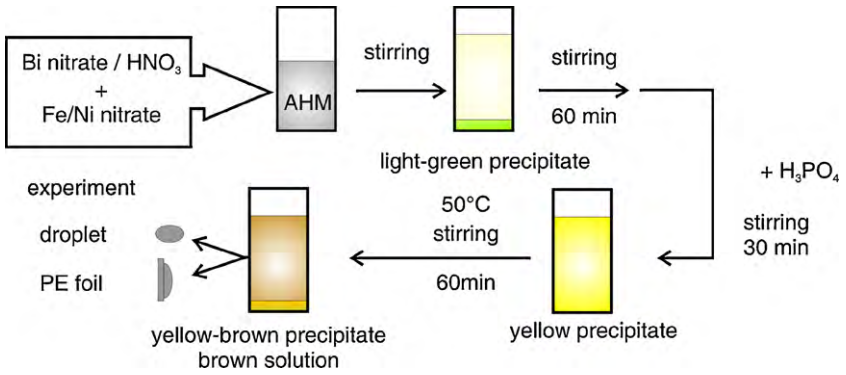

Fig. 1. Preparation flow chart.

kinetics of pharmaceutical proteins suggest that an acoustic levitator can be used as a model system for spray drying [6,8].

Previously, we have used an acoustic levitator to investigate the crystallization processes of small molecules and proteins [9–11]. The objective of this study is to explore, whether the spray drying process of a typical catalyst synthesis mixture containing AHM, Ni, Fe and Bi nitrate, HNO_3 and H_3PO_4 can be modelled and monitored by trapping slurry droplets in an ultrasonic levitator. To gain a deeper insight into the drying process, *in situ* X-ray scattering investigations were performed.

2. Experimental

2.1. Sample preparation

A typical slurry used in the experiments was prepared as already described [3] and is displayed in Fig. 1. The composition of the mixture was chosen to mimic the complexity of catalysts typically used. 25 mL aqueous solution of 11.63 g $Ni(NO_3)_2{\cdot}6H_2O$, 4.04 g $Fe(NO_3)_3{\cdot}9H_2O$ and 4.86 g $Bi(NO_3)_3{\cdot}5H_2O/HNO_3$ were added to 24.72 g AHM in 75 mL H_2O. After one hour stirring 2.5 mL 85 wt.% H_3PO_4 were added. This slurry was stirred for further 30 min and afterwards heated up to 50 °C. At this temperature the mixture was stirred for one hour.

2.2. In situ experiments

In a typical experiment one droplet of this solution with a volume of 2.5 μL was directly hand-injected into the ultrasonic levitator by means of a microlitre pipette (0.5–10 μL, Eppendorf, Germany) and irradiated by the X-ray beam (100 μm in diameter, $E = 11.94$ keV, $\Delta E/E \approx 10^{-4}$, $\lambda = 0.10386$ nm). Acoustic levitation allows a stable positioning of sample volumes from 5 nL to 5 μL without influence from solid container walls. An ultrasonic trap (Tec5, Oberursel, Germany) was implemented at a micro focus beamline (Fig. 2, further information on the beamline can be found in ref. [12]). Applying this setup, the monitoring of tiny sample amounts in an acoustically levitated droplet is possible. Scattered intensities were collected 20 cm behind the sample with a two-dimensional X-ray detector (MarMosaic, CCD 3072 × 3072 pixel and a point spread function width of about 100 μm). The same experiment was repeated on sessile droplets deposited on PE foil. A turnable microscope was used in its in-beam-position to align the sample precisely at the X-ray micro spot. During the experiment the sample was observed in an off-beam-position. Interference from scattered radiation leads to smooth diffraction rings around the beam axis (Debye–Scherrer rings [13]). These scattering images were converted by algorithm of the software FIT2D [14] into diagrams of scattered intensities as a function of the scattering vector q, defined as $q = 4\pi/\lambda \sin\theta$, where 2θ is the scattering angle between incident and scattered photons and λ the wavelength. Due to the small incident beam diameter no mathematical correction of the experimental scattering function was needed. In the case of a levitated droplet, the scattering from pure solvent was used to estimate the background contribution.

3. Results and discussion

In Fig. 3 the recorded scattering curves of a levitated droplet of slurry are shown. Each pattern was collected with an irradiation time of 10 s during 60 min of levitation. Fig. 3 shows the first 24 min of levitation, starting from the top to the bottom curve.

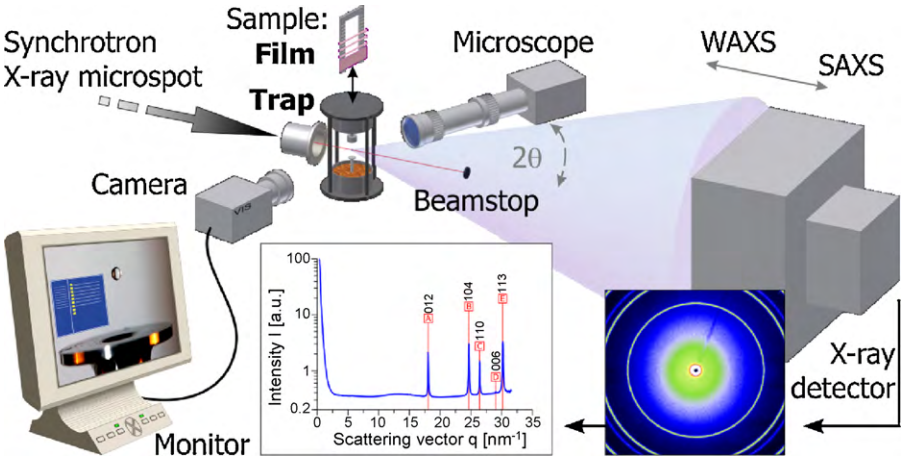

Fig. 2. Experimental implementation of an acoustic levitator (trap) for X-ray scattering. Switchable sample holders (a) trap, and (b) film.

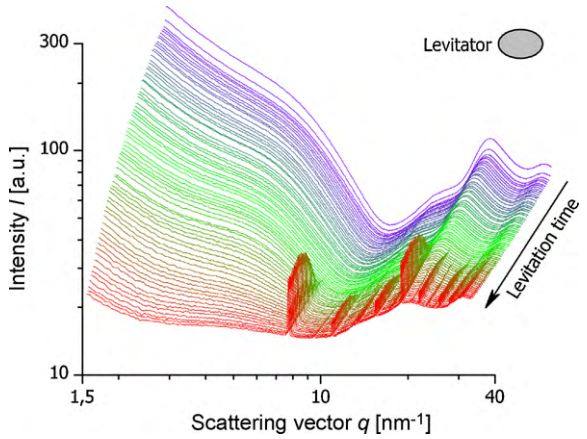

Fig. 3. Scattering curves of the Mo/Ni/Fe/Bi slurry phase in a levitated droplet collected every 20 s (top to bottom).

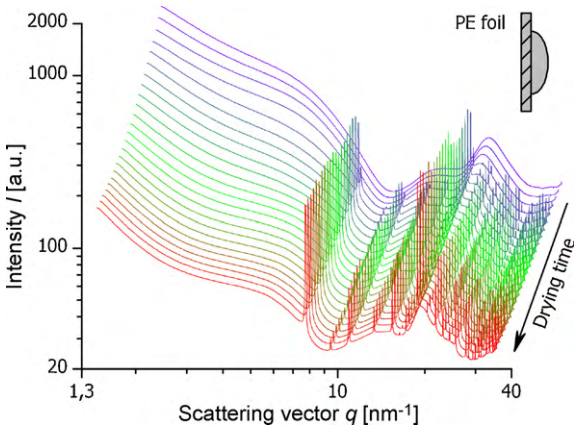

Fig. 5. Scattering curves of the Mo/Ni/Fe/Bi slurry phase in a droplet positioned on PE foil collected every 80 s (top to bottom).

Afterwards the diffraction patterns remain unchanged. Throughout the experiment the volume of the droplet decreases due to the evaporation of water (see Fig. 4). The absence of Bragg reflections in the first part of the experiment indicates that the formation of crystalline phases is hampered, while a broad maximum at $q = 20\ nm^{-1}$ is attributed to the amorphous scattering signal of the aqueous solution (see Fig. 4, inset A). The first scattering curves exhibit strong scattering signals in the region of $q < 7\ nm^{-1}$ (SAXS), indicating aggregated particles. With increasing levitation time the scattering intensities for low q decrease and a shoulder at $q = 5\ nm^{-1}$ is formed. After approximately 15 min, sharp peaks signify the formation of crystalline material. At this point the volume of the droplet is decreased from 2.5 μL to 1 μL (see Fig. 4, inset B). All reflections appear split and coalesce continuously to a single reflection. This effect is due to the formation of the crystals at the air/water interface on the droplets surface. The experimental implications are described elsewhere in detail [15]. The minimal droplet volume of 0.5 μL was reached after 30 min. The sharpness and the intensity of the Bragg reflections remain unchanged, whereas the intensity of the broad halos at approximately 15 nm^{-1} and 20 nm^{-1} increases, indicating the formation of amorphous structures.

For comparison, in further experiments, droplets were deposited on a polyethylene (PE) foil. Irradiating the droplet through the film with an exposure time of 60 s, scattering curves were recorded during 32 min of evaporation (see Fig. 5). The recorded scattering curves are comparable to those obtained from experiments using a levitated droplet (cf. Fig. 3). However, the crystallization starts already after 4 min compared to 15 min using the levitated droplet. A splitting of the reflections cannot be observed but their positions are shifted continuously to larger q-values (e.g. 33.59–33.65 nm^{-1}), implicating an increasing sample to detector distance. In accordance with the situation in the levitated droplet, the crystallization starts at the water/air interface. This moves continuously in the direction of the sample support during the evaporation of solvent [16].

The final diffraction patterns were carefully corrected for amorphous background scattering and compared with the pattern of the product after spray-drying, measured under similar conditions. The diffraction patterns of dried samples derived from the different experiments described above were compared with a diffraction pattern from a spray-drying experiment and are in good accordance. The structure was indexed to a cubic crystal system with the lattice constant of 11.67 Å. As depicted, the obtained data are comparable with the PDF database entry 43-314 [17] of $(NH_4)_3(PMo_{12}O_{40})\cdot xH_2O$ where the intensity was normalized to the 222 reflection at $q = 18.6\ nm^{-1}$ to a value of 100 (Fig. 6). The crystal structure consists of Keggin-type ions in which some of the Mo positions are substituted by Fe or Bi, respectively. Differences in the crystal growth between both experimental setups could be deduced from the evolution of the Bragg reflections. From the peak width of Bragg reflections a value for the mean crystal dimension

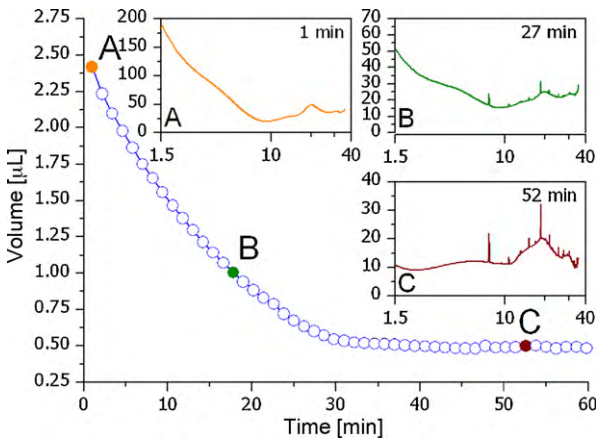

Fig. 4. Decrease in the volume of an evaporating slurry droplet during a typical experiment. Different stages of the crystallization are indicated in the insets where the graphs represent scattering intensity [a.u.] *vs* scattering vector [nm^{-1}].

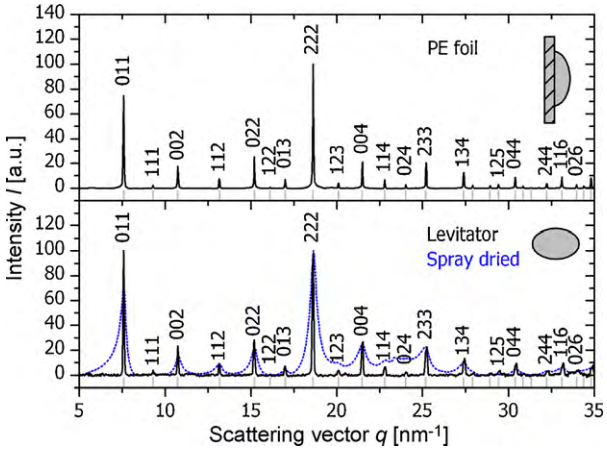

Fig. 6. Scattering curves of the final dried slurry phase from the PE foil (upper part) and from the levitator (lower part) are compared with diffraction data (delta peaks, grey) of $(NH_4)_3(PMo_{12}O_{40})\cdot xH_2O$ and Miller indices. The blue dotted curve in the lower row of the diagram denotes the scattering curve of the spray dried sample. (For interpretation of the references to color in this figure legend, the reader is referred to the web version of the article.).

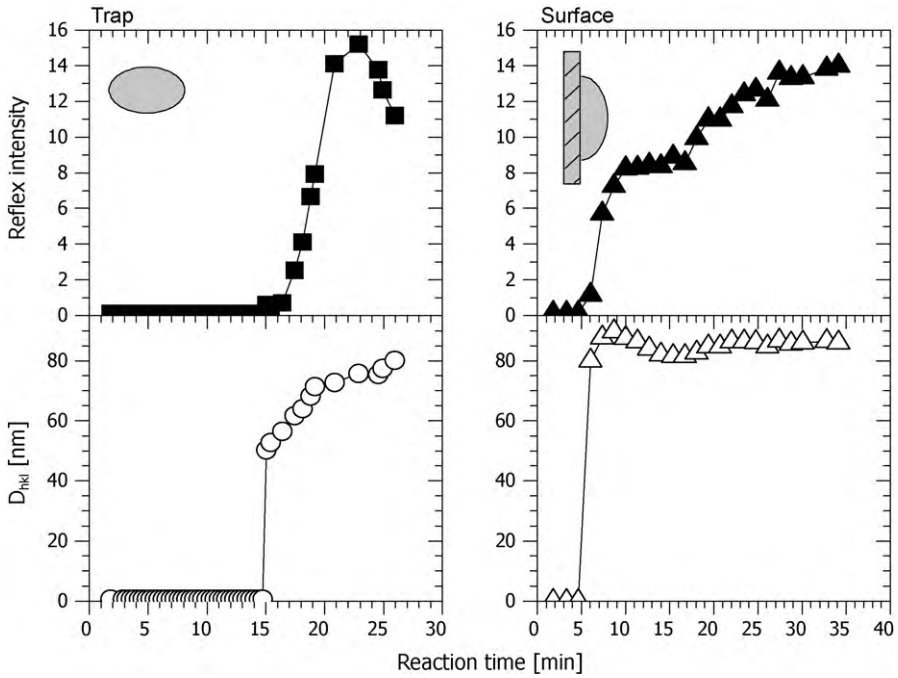

Fig. 7. Intensity of Bragg (0 1 1) reflections (filled) and calculated crystallite size (hollow symbols) from levitated sample and sample on PE foil. The error bars of data points are in the range of the symbol size.

can be calculated according to the Scherrer equation [18,19]. Fig. 7 summarizes the calculated mean sizes of crystallites based on a representative reflection (0 1 1) at $q = 7.7\ nm^{-1}$ and maximal intensity of Bragg reflections for the levitated droplet and the droplet on the PE foil. The reflection intensity shows the same progress over time for the maximum of the reflections and the integral of the peak curve. In the case of the experiments carried out in the acoustic levitator, as soon as Bragg reflections occur, all reflection intensities (cf. Fig. 3) increase to a maximum at 23 min and continue decreasing in maximum intensity as well as in integral value of reflections shape. The corresponding mean size of crystallites increases continuously from 40 nm to 80 nm. Consequently, a decreasing number of crystallites with growing dimensions have to be concluded. These observations are in accordance with a continuous decrease in scattering intensity at smallest scattering vectors in the SAXS-region, indicating a lower amount of particles. This is in accordance with the well-known Ostwald ripening [20]. The results concerning the crystal growth in the droplet on the PE foil differ. In the latter case, distinct Bragg reflections were recorded after 5 min. The height of these reflections increases rapidly by a factor of 10 within 5 min and continues growing gradually until the end of experiment. At the beginning, the mean crystallite dimension can be estimated to 80 nm, which is twice the value of those obtained in the experiment using a levitated droplet. Afterwards, the value converges to 86 nm.

For comparison, the diffraction pattern of a sample obtained from a spray-drying experiment (same constitution, temperature of cyclone 118 °C, drying chamber 200 °C) was included in Fig. 6. This sample consists of the same phase but a significantly lower crystallite size of about 12 nm was detected, which can be explained by the fast rate of drying during this process.

4. Conclusions

The tiny compartment of an acoustically levitated droplet was successfully used for the structural investigation of the drying process of a complex molybdate precursor slurry and compared with a droplet positioned on PE foil. It could be shown that the sample environment had no influence on the crystal structure. The same crystallization product with cubic crystal structure like $(NH_4)_3(PMo_{12}O_{40})\cdot xH_2O$ has been obtained independent on the drying procedure (acoustically levitated droplet *vs* droplet positioned on PE foil *vs* spray-died product). However, it was found by *in situ* monitoring using synchrotron X-ray analysis, that the crystal growth differs markedly. For the droplets fixed on the PE foil the amount of large crystallites of about 80 nm increases during the drying, whereas for the levitated droplets the crystallite size increases, while the number reaches a maximum. In contrast, a much smaller mean crystallite size of only 12 nm is detected in the respective spray-dried sample. This suggests that the different water evaporation rate in the three procedures has a crucial influence on the mean crystallite size. Controlling the water evaporation rate in the ultrasonic levitator could, thus, open interesting opportunities for designing dedicated slurry drying procedures resulting in catalyst precursors with tailored crystallite size, provided that those procedures are transferable to industrial praxis. However, despite differences in droplet size, temperature and drying speed, the acoustic levitation seems to be a powerful tool to derive relevant structural data about the crystallization during a mimicked spray drying process. Using small sample amounts (4–10 μL) variation of the temperature, humidity and composition of the droplets allows further insights into the crystallization process for catalytically relevant materials. These findings can be transferred and enable an optimization of the drying process.

References

[1] G. Centi, F. Cavani, F. Trifirò, Selective Oxidation by Heterogeneous Catalysis, Kluwer Academic Publishers, New York, 2001.
[2] F. Schüth, Chemie Ingenieur Technik 77 (2005) 1399.
[3] U. Bentrup, J. Radnik, U. Armbruster, A. Martin, J. Leiterer, F. Emmerling, A. Brückner, Top. Catal. 52 (2009) 1350.
[4] M.M. Lin, Appl. Catal. A: Gen. 207 (2001) 1.
[5] D. Sen, O. Spalla, O. Tache, P. Haltebourg, A. Thill, Langmuir 23 (2007) 4296.
[6] H. Schiffter, G. Lee, J. Pharm. Sci. 96 (2007) 2274.
[7] S. Santesson, S. Nilsson, Anal. Bioanal. Chem. 378 (2004) 1704.

[8] H. Schiffter, G. Lee, J. Pharm. Sci. 96 (2007) 2284.
[9] J. Leiterer, W. Leitenberger, F. Emmerling, A.F. Thünemann, U. Panne, J. Appl. Crystallogr. 39 (2006) 771.
[10] J. Leiterer, F. Emmerling, U. Panne, W. Christen, K. Rademann, Langmuir 24 (2008) 7970.
[11] F. Delissen, J. Leiterer, R. Bienert, F. Emmerling, A.F. Thünemann, Anal. Bioanal. Chem. 392 (2008) 161.
[12] O. Paris, C. Li, S. Siegel, G. Weseloh, F. Emmerling, H. Riesemeier, A. Erko, P. Fratzl, J. Appl. Crystallogr. 40 (2007) S466.
[13] P. Debye, P. Scherrer, Physikalische Zeitschrift 17 (1916) 277.
[14] A.P. Hammersley, S.O. Svensson, M. Hanfland, A.N. Fitch, D. Hausermann, High Press. Res. 14 (1996) 235.
[15] S.E. Wolf, J. Leiterer, M. Kappl, F. Emmerling, W. Tremel, J. Am. Chem. Soc. 130 (2008) 12342.
[16] R.D. Deegan, O. Bakajin, T.F. Dupont, G. Huber, S.R. Nagel, T.A. Witten, Nature 389 (1997) 827.
[17] Powder Diffraction File (PDF), The International Centre for Diffraction Data (ICDD), 2008.
[18] P. Scherrer, Bestimmung der Grösse und der inneren Struktur von Kolloidteilchen mittels Röntgenstrahlen, Nachrichten von der Gesellschaft der Wissenschaften, vol. 2, Göttingen, 1918, p. 98.
[19] H.P. Klug, L.E. Alexander, X-ray Diffraction Procedures: For Polycrystalline and Amorphous Materials, Wiley-Interscience, 1974.
[20] W. Ostwald, Z. Phys. Chem. 22 (1897) 289–330.